Journal of Applied Mechanical Engineering
ISSN: 2168-9873

Toms, J Appl Mech Eng 2015, 4:3
DOI: 10.4172/2168-9873.1000169

Research Article Open Access

Large-eddy Simulation of Flow Over a Backward Facing Step: Assessment of Inflow Boundary Conditions, Eddy Viscosity Models and Wall Functions

Benjamin A Toms[1-3]*

[1]Summer Undergraduate Research Fellow, Fire Research Division, Engineering Laboratory, National Institute of Standards and Technology, Gaithersburg, Maryland, 20899, USA
[2]Department of Civil Engineering and Environmental Sciences, University of Oklahoma, Norman, Oklahoma, 73019, USA
[3]Department of Atmospheric and Geographic Sciences, University of Oklahoma, Norman, Oklahoma, 73019,USA

Abstract

Large-eddy simulation (LES) of turbulent flow over a backward facing step is studied to test the influence of grid resolution, inlet turbulence, wall boundary treatments, and eddy viscosity models. The computational results are validated with experimental data. A grid resolution with 10 cells spanning the step height adequately models the flow, although a doubling of resolution results in the realization of smaller scale kinematic features. The inlet turbulence conditions are determined to be the most significant contributor to downstream flow evolution. Reattachment length is found to be strongly dependent on the magnitude of the inlet root-mean-square velocity. The choice of eddy viscosity model is found to have negligible influence, while the no-slip condition and an LES log-law-based wall function performed similarly for the given flow.

Keywords: Large-eddy simulation; Backward facing step; Turbulent boundary conditions; Wall functions; Computational fluid dynamics

Introduction

The Fire Dynamics Simulator (FDS) is a large-eddy simulation (LES) code used to model low-mach flows driven by combustion heat release and buoyancy [1-2]. FDS has recently been applied to urban canopy modeling [3] and wind engineering. As such, it is important to study geometrically influenced flows, including the appropriate specification of boundary conditions and resultant downstream flow evolution.

The backward facing step is a commonly used geometry in the study of turbulent flows.Extensive research on this flow has been conducted using direct numerical simulation (DNS), Reynolds-Averaged Navier-Stokes (RANS), and LES. DNS has offered computational results most consistently resemblant of experimental data (e.g. the comparison of LES results of Panjwani et al. [4] to the DNS results of Le et al. [5] and experimental results of Jovic and Driver [6]. However, studies performed by authors such as Saric et al. [7] have suggested optimally conditioned LES code may simulate the flow as accurately as DNS.

The backward facing step has been utilized to study such cases as wall heat transfer, pressure drops following kinematic interaction with complex geometry, and influence of geometry on turbulence related mixing of fluid properties [8-10]. Although the foundation of research relating to the backward facing step is meritorious, parametric study focusing on influence of commonly varied computational domain characteristics (e.g. wall boundary conditions, inlet turbulence, etc.) is limited. The number of studies using FDS is further limited. As such, the goal of the present work is to confirm the capability of FDS to model geometrically complex flows and to assess the importance of boundary conditions and subgrid models on the results.

Le et al. [5] first modeled flow over a backward facing step using DNS with a Reynolds number of 5,100. To verify the results, Jovic and Driver (J and D) [6] supplemented the DNS simulation with an identically proportioned wind tunnel experiment. Together, the data sets from these two studies have provided the baseline for analysis of recent simulations of flow over a backward facing step.

Panjwani et al. [4] used LES to study the influence of eddy viscosity subgrid-scale (SGS) modeling, discretization schemes, and grid refinement on LES accuracy in comparison to the DNS of Le et al. [5]. Effects of SGS modeling were determined to be minimal, whereas the discretization schemes were found to have a substantial impact.

Aider et al. [11] studied the influence of inlet turbulent boundary conditions on downstream flow characteristics. Inlet turbulence boundary conditions were found to have significant impact on flow development. These results supplement those of Isomoto and Honami who concluded the maximum turbulence intensity to have an inverse relationship with reattachment length, and are further confirmed by Dol et al. who determined integration of a pulsation frequency on inlet kinematics influence downstream eddy development. Namely, Aider et al. [11] found higher values of root-mean-square (RMS) velocity led to a more rapid destabilization of the shear layer that develops downstream of the step. This resulted in a reduction in reattachment length and a faster redevelopment of the mean stream wise velocity profile, $\overline{u}(z)$. (Throughout this document, an over line is used to denote a mean quantity.)

Sarwar et al. [12] used FDS to compare SGS eddy viscosity models. The constant Smagorinsky model [13] performed the best, although Germano [14,15] and Deardorff [16] models, are nearly equivalent in accuracy, were found to perform better than the Vreman model [17]. To avoid explicit specification of inlet turbulence conditions, Sarwar et al. [12] created an extremely long inlet section to allow turbulence to develop. One of the goals of the present study is to show that synthetic turbulent inflow boundary conditions can be successfully used to greatly reduce the size of the inlet domain and hence the calculation

***Corresponding author:** Benjamin A Toms, Department of Civil Engineering and Environmental Sciences, University of Oklahoma, Norman, Oklahoma, 73019, USA, Tel: 303 483 8268; E-mail: benatoms@gmail.com

Received May 22, 2015; **Accepted** June 19, 2015; **Published** June 26, 2015

Citation: Toms BA (2015) Large-eddy Simulation of Flow Over a Backward Facing Step: Assessment of Inflow Boundary Conditions, Eddy Viscosity Models and Wall Functions. J Appl Mech Eng 4: 169. doi:10.4172/2168-9873.1000169

cost.

For the present study, grid resolution, inlet turbulence definition, SGS eddy viscosity modeling, and wall models are analyzed using FDS 6.1.0 to determine the most influential variables on flow development. Simulations with varying grid resolutions are compared to the J and D experimental data. Using adequate grid resolution, the effects of inlet RMS velocity magnitude are studied. The effectiveness of the Deardorff and dynamic Smagorinsky SGS eddy viscosity models are compared. Influences of the wall condition are determined through a comparison of an LES log-law-based wall function with the no-slip and free-slip wall conditions.

Methodology

Computational domain

A schematic view of the computational domain is provided in Figure 1. The dimensions of the channel, based on step height h=.0098 m, are defined as follows: length of channel, $L_{x=}$24 h; length of inlet, L_i=4 h; width of channel, L_y=4 h; height of channel inlet, $L_{iz=}$5 h; height of channel post-step, L_z=6 h. The expansion ratio, defined as L_{iz}/L_z, is thus 1.2. The inlet is split into three sub-inlets to permit localized variation of inlet turbulence. The simulation uses a step-height Reynolds number of 5,100 based on a free stream velocity of $U_{0=}$7.2 m/s.

To give the reader a qualitative sense of the flow field, Figure 2 presents instantaneous contours of velocity magnitude. For quantitative results, virtual measurement devices are placed throughout the channel to collect data relating to flow characteristics such as velocity, turbulence RMS velocity, and friction velocity. These virtual measurement devices are placed into lines—four vertical and one horizontal-with a device in the volumetric center of each grid cell. A vertical line device is placed within the inlet region at a location of x=−3h, and three line devices are placed in the post-step region at locations of 4h, 6h, and 10h. The post-step vertical line devices are placed accordingly to sample the recirculation, reattachment, and recovery regions. A horizontal array of virtual anemometers is used to sample velocity data directly adjacent to the bottom wall of the channel in the post-step region (0h to 20h).

Boundary conditions

The inlet $\overline{u}(z)$ profile is established using experimental data provided by J and D [6], while $\overline{v}(z)$, $\overline{w}(z)$, and inlet free-stream

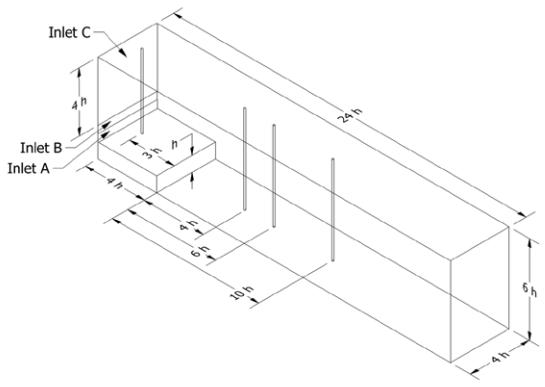

Figure 1: Schematic of the channel computational domain. Virtual measurement devices are denotedby the vertical lines at x=−3 h, 4 h, 6 h, 10 h. All three inlet sections utilize a mean velocityprofile set to match the mean streamwise profile from the J and D experimental data at x=−3 h.Varying degrees of inlet turbulence are superimposed on the mean velocity for inlets A andB, as shown in Table 1.

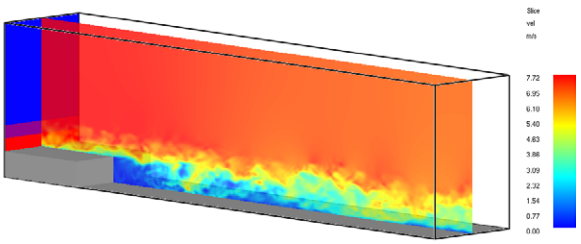

Figure 2: Instantaneous contours of velocity magnitude.

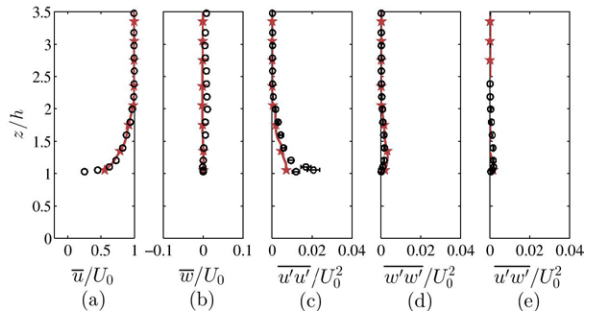

Figure 3: Flow profiles at x/h=3.0 (near the inlet) of (a) normalized $\overline{u}$(z), (b) normalized $\overline{w}$(z), (c)normalized $\overline{u'u'}$, (d) normalized $\overline{w'w'}$, (e) normalized $-\overline{u'w'}$. Symbols: –⋆ –, FDS profile; ◦, J and Dexperimental data.

turbulence are set to zero. Based on the $\overline{u}(z)$ profile provided by J and D, the pre-step boundary layer depth is equivalent to h [6]. The summed vertical span of the two bottom inlets is equivalent to the inlet boundary layer height. Turbulent eddies are injected using the Synthetic Eddy Method of Jarrin [18]. Eddies are injected at random locations in the bottom two inlets, advected with the flow over a distance equal to the maximum eddy length scale l_0, and recycled at the inlet. The inlet maximum eddy length scale, number of eddies, and RMS velocity is pre-defined. The Reynolds stress and eddy length scale are assumed to be isotropic.

The boundary conditions for velocity and pressure on the top of the domain are "mirror", that is, zero normal gradients. The span wise boundaries are periodic. The outlet boundary is "open", meaning the outlet pressure is specified based on the direction of the flow [1].

In an attempt to replicate the J and D experiment, the inlet boundary conditions are modified to resemble the experimental inlet data as closely as possible. This is complicated by inlet turbulence profile limitations of FDS. Currently, FDS allows specification of turbulence parameters unique to each inlet (a "vent" in FDS nomenclature), but does not allow direct designation of an inlet turbulence profile. The turbulence parameterization that results in kinematic profiles and turbulence statistics most representatives of J and D data is used as the baseline case throughout the study. The RMS velocity is 1.0 m/s for the bottom inlet (Inlet A), 0.5 m/s for the middle inlet (Inlet B), and 0.0 m/s for the top inlet (Inlet C). For both inlets A and B, the maximum eddy length scale is 0.03 m and number of injected eddies is 100. The number of eddies is set high enough to ensure correct inlet statistics. Figure 3 compares J and D data to the resultant inlet mean velocity and turbulence statistics profiles using a grid resolution of $h/\delta z$=10.

Of note, J and D provided error associated with the experimental measurements – these values have been incorporated as error bars

Case Number	Resolution (h/δz)	Inlet RMS Velocity (m/s)		Eddy Viscosity Model	Wall Condition	Reattachment Length (x/h)
		A	B			
1(i)	5	1	0.5	Deardorff	LES log- law	9.9
2(i)	10					5.95
3(i)	20					5.275
1(ii)	10	0	0	Deardorff	LES log-law	11.25
2(ii)		1	1			5.55
3(ii)		1	0.5			5.95
1(iii)	10	1	0.5	Deardorff	LES log-law	5.95
2(iii)				dynamic Smag		5.95
1 (iv)	10	1	0.5	Deardorff	LES log-law	5.95
2(iv)					No-slip	6.05
3(iv)					Free-slip	5.85

Table 1: Parameter specifications for each case. The experimentally determined reattachment length from Jovic and Driver [7] is 6.00 ± 0.15. Roman numeral Table 1 identification for each respective study: (i) grid resolution; (ii) inlet turbulence modification; (iii) turbulence model; (iv) wall condition.

into subsequent plots. J and D designated the error associated with velocity measurements, Reynolds stress and turbulence intensity measurements, and friction coefficients as, respectively, 2%, 15%, and ± 0.0005.

Results and Discussion

Grid resolution

Grid resolutions of $h/\delta z$= 5, 10, and 20 are compared to determine the minimum grid resolution requirement. Case 3(ii) is used as the baseline case for grid resolution analysis (Table 1). For validation, in the following sections the longitudinal friction coefficient and pressure coefficient profiles, mean velocity profiles, and turbulence intensity and Reynolds stress profiles are compared to J and D experimental data [6].

Friction coefficient and reattachment length: The reattachment length is defined as the location of zero vertical gradient of longitudinal velocity at the wall: $\partial\overline{u}/\partial z|_{z=0}=0$. If two locations of $\partial\overline{u}/\partial z|_{z=0}=0$ occur due to a secondary recirculation region [19], the point farther from the step is designated the reattachment point. The reattachment lengths for the 5, 10, and 20 resolution cases are, respectively, x/h=9.9, 5.95, 5.275. Averaged flow quantities have been shown to be dependent on reattachment length [20]. Therefore, due to the significant difference between the h/δz=5 and J and D reattachment lengths, all statistics are poorly represented by the lowest resolution case.

The friction coefficient is defined as

$$C_f = \frac{\tau_w}{\frac{1}{2}\rho U_0^2} \tag{1}$$

where

$$\tau_w = \mu \frac{\partial \overline{u}}{\partial z}|_{z=0} \tag{2}$$

and is therefore proportional to the vertical gradient of $\overline{u}$ at the wall. Figure 4a shows post-step longitudinal C_f profiles for each resolution. The $h/\delta z$=10 case correctly displays the qualitative characteristics of the longitudinal C_f profile, but does not realize the magnitude of the sharp dip within the recirculation region. In the recirculation region, the magnitude of C_f is most accurately captured by the $h/\delta z$=20 case, although the recirculation length is too short and thus the qualitative characteristics are skewed toward the step. The $h/\delta z$=5 case incorrectly models both the qualitative and quantitative characteristics of the C_f longitudinal profile [21].

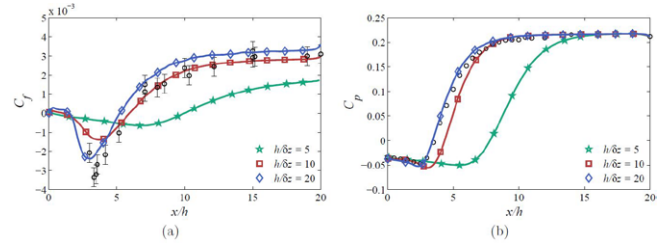

Figure 4: Grid resolution comparison (Cases 1(i)-3(i)) for longitudinal profiles of (a) frictioncoefficient, and (b) pressure coefficient. Symbols: – ⋆ –, h/δz=5; –□–, h/δz=10; –◊–, h/δz=20;◦, J and D experimental data. Note, error of experimental measurements has been denoted byerror bars.

There is a direct relationship between grid resolution and C_f magnitude within the recirculation region. This is likely the result of enhanced sampling of the near-wall region with increased resolution. For the given computational domain, DNS simulations have shown deviations from the LES log-law viscous sub layer depth (z^+ <12) [5], necessitating enhanced grid resolution to correctly resolve the near-wall $\overline{u}(z)$ profile. The $h/\delta z$= 20 case is the only resolution capable of sampling data within both the viscous sub layer and buffer layer in the mean.

Pressure coefficient: The coefficient of pressure is defined as

$$C_p = \frac{p - p_0}{\frac{1}{2}\rho U_0^2} \tag{3}$$

Where p is the pressure and p_0 is the background pressure. The pressure coefficient is thus proportional to localized pressure perturbations. Figure 4b presents the computational C_p data compared to J and D data.

The $h/\delta z$=5 case performs poorly. The $h/\delta z$=10 case is qualitatively correct, but results in the pressure coefficient profile being shifted downstream relative to the J and D data. The $h/\delta z$=20 case is within 5% of the J and D data at the reattachment location. However, the recirculation length for the $h/\delta z$=20 case is shorter than that of J and D, so the quantitative accuracy in the stream-wise extremity of the recirculation region is questionable. All grid resolutions result in similar maximum magnitude of pressure perturbation within the recirculation region.

Wall-normal velocity and Reynolds stress profiles: Figure 5 shows wall-normal velocity and Reynolds stress profiles for the grid resolution study. The h/δz=5 case performs poorly for all kinematic variables and will not be discussed further. The profile of $\overline{w}(z)$ at h/δz=20 matches J and D data more closely than the h/δz=10 case. The $\overline{u}(z)$ profiles for both cases identically match J and D data.

With increasing resolution, the spike in $\overline{u'u'}$ near the wall is better captured. The $\overline{u'u'}$ values of the $h/\delta z$= 10 and 20 cases are within the margins of error of the J and D data, except for within the recovery region. The $\overline{w'w'}$ and $\overline{u'w'}$ (Reynolds stress) values are too large in both cases.

Minimum grid resolution requirement: The h/δz=5 grid resolution performs poorly. The h/δz=10 grid resolution adequately models the qualitative characteristics of the flow. Although the h/δz=10 and h/δz=20 grid resolution simulation results differ quantitatively, both cases are within experimental error of data provided by J and D. Therefore, the h/δz=10 grid resolution is adequate both qualitatively and quantitatively, and is utilized throughout the remainder of the study.

Inlet turbulence modification

The significance of inlet turbulence is studied through a comparison of a set of inlet turbulence cases. Refer to Table 1 for parameterizations of each case. In the first case, no turbulence is injected. For the second case, turbulence of the same RMS velocity magnitude is injected into both lower inlets. For the third case, the RMS velocity magnitude of the middle inlet (inlet B) is half that of the bottom inlet (inlet A). These cases are henceforth referred to as the no turbulence, two inlet, and three inlet cases respectively. Neither the maximum eddy length scale nor the number of injected eddies is varied.

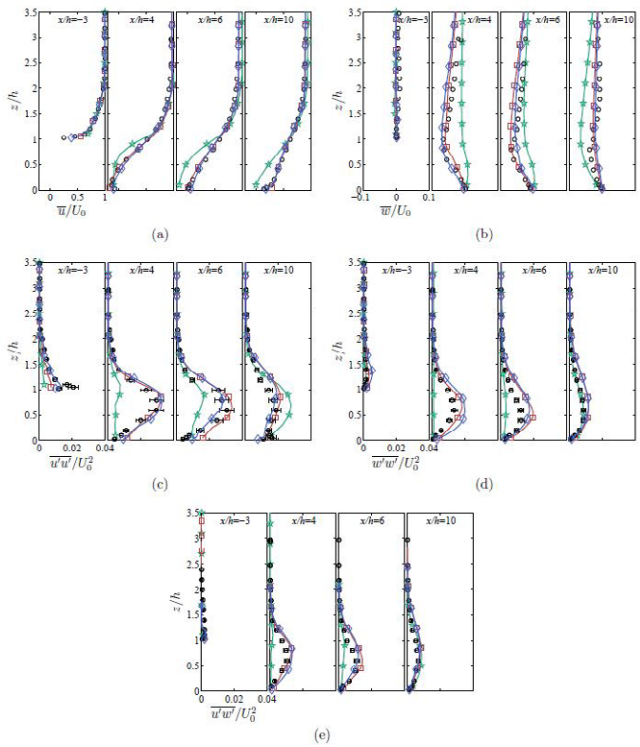

Figure 5: Grid resolution comparison (Cases 1(i)-3(i)): (a) normalized $\overline{u}$(z) profiles; (b) normalized$\overline{w}$(z) profiles; (c) normalized $\overline{u'u'}$; (d) normalized $\overline{w'w'}$; (e) normalized $-\overline{u'w'}$ Reynolds stress.Symbols: –⋆ –, h/δz=5; –□–, h/δz=10; –◊–, h/δz=20; ◦, J and D experimental data. Note, error ofexperimental measurements has been denoted by error bars.

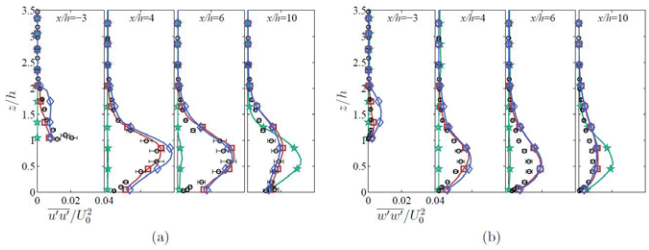

Figure 6: Inlet turbulence RMS velocity comparison (Cases 1(ii)-3(ii)): (a) normalized $\overline{u'u'}$; (b) normalized $\overline{w'w'}$. Symbols: – ⋆ –, no turbulence; –□–, two inlet; –◊–, three inlet; ◦, J and D experimental data. Note, error of experimental measurements has been denoted by errorbars.

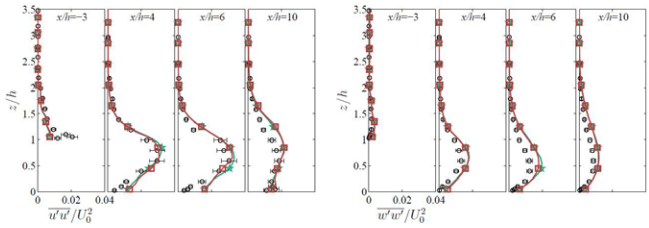

Figure 7: Turbulence model comparison (Cases 1(iii)-2(iii)): (a) normalized $\overline{u'u'}$; (b) normalized $\overline{w'w'}$.Symbols: –⋆ –, Deardorff; –□–, dynamic Smagorinsky; ◦, J and D experimental data. Note, error of experimental measurements has been denoted by error bars.

The reattachment lengths for the no turbulence, two inlet, and three inlet turbulence modification cases are, respectively, x/h=11.25, 5.55, 5.95. This aligns with previous research suggesting inlet RMS velocity magnitude and reattachment length are inversely related [11]. The no turbulence case drastically overestimates the reattachment length, and therefore significantly differs from J and D data for all studied flow variables.

The longitudinal C_f and C_p profiles for the two and three inlet turbulence cases are similar, although the recirculation region associated pressure gradient is larger for the three inlet case. Figure 6 shows $\overline{u'u'}$ and $\overline{w'w'}$ values for all three cases. As discussed in Sec. 3.1.3, the $\overline{u'u'}$ values for the three inlet case falls within experimental error bounds of the J and D data, except within the recovery region. The two inlet case exhibits excessive $\overline{u'u'}$ values within the recirculation and recovery regions. Both cases exhibit excessive $\overline{w'w'}$ and $-\overline{u'w'}$ values throughout the channel, although the three inlet case is more accurate.

Turbulence model

In this section, the Deardorff and dynamic Smagorinsky eddy viscosity models [1] are compared. Of note, in the first layer of cells adjacent to the wall, FDS uses the constant Smagorinsky model with Van Driest damping [1]. This is to avoid inconsistencies related to test filtering operations near the wall. The results are shown in Figure 7.

There is no distinguishable difference between the post-step C_f profiles, reattachment lengths, C_p profiles, or $\overline{u}(z)$ profiles. The reattachment length for both models is x/h=5.95. All subsequently

discussed differences between the models are small. The dynamic Smagorinsky model shows more negative w within the recirculation region and within the region near the reattachment point. Additionally, the turbulence intensity within the recirculation region is larger for the dynamic Smagorinsky model than for the Deardorff model. In contrast, the Deardorff model exhibits larger turbulence intensity within the recirculation region. Neither model captures the spike in $\overline{u'u'}$ near the wall at the inlet.

Aside from these small differences, the Deardorff and dynamic Smagorinsky eddy viscosity models result in similar flow characteristics.

Wall model

The LES log-law wall model, no-slip wall condition, and free-slip wall condition are also compared (Figure 8). For the LES log-law wall model, the stream wise velocity component in the grid cell closest to the wall, $u(\delta z/2)$, is sampled from the following piecewise function:

$$u^+ = \begin{cases} z^+ & for\, z^+ < 12 \\ \frac{1}{\kappa}\ln\left(z^+\right) + B & for\ z^+ \geq 12 \end{cases} \quad (4)$$

Where $u^{+=}u/u^*$ and $z^{+=}z/\delta_v$. Here, u^* is friction velocity and δ_v is the viscous length-scale; κ= 0.41 is the von Kármán constant and B=5.2 for a smooth wall.

For the no-slip wall condition, wall-normal gradients of stream-wise velocity are calculated using a finite difference. For the free-slip wall condition, the gradient of stream-wise velocity in the wall-normal direction is zero at the wall and hence there is no stress at the wall.

The reattachment points for the log-law model, no-slip condition, and free-slip condition are x/h=5.95, 6.05, 5.85 respectively. As shown in Figure 9a, both the LES log-law model and no-slip condition C_f profiles qualitatively match that of J and D. However, the LES log-law model results are more accurate. Neither model captures the dip in C_f within the recirculation region. The free-slip C_f is zero throughout the channel due to $\partial\overline{u}/\partial z|_{z=0} = 0$. There is no discernible difference in C_p profiles between the LES log-law model and nonslip condition, although the free-slip condition results in an excessive negative pressure perturbation within the recirculation region (plot not shown).

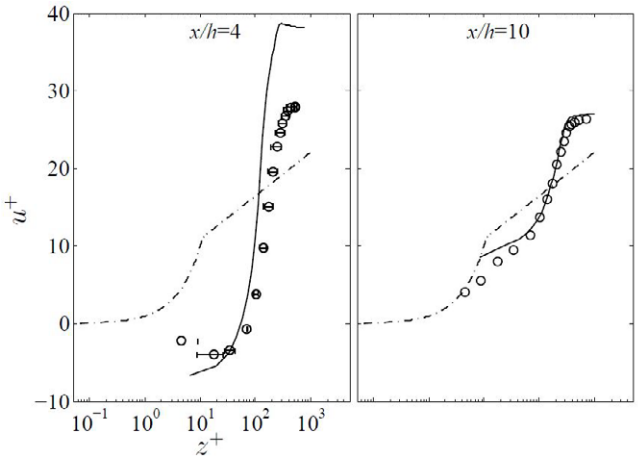

Figure 8: Vertical u+ profiles within the (a) recirculation and (b) recovery regions. Symbols: —, computational profile; -·-, log-law profile; ◦, J and D experimental profile. Note, a grid resolutionof h/dx =10 and the LES log-law wall model were used for the computational profile.

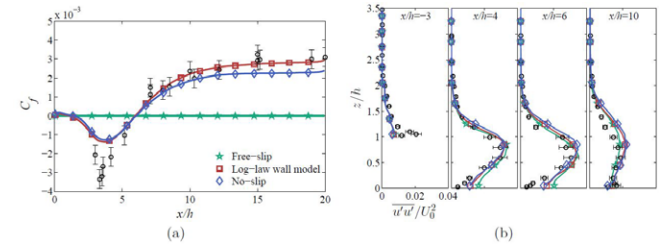

Figure 9: Wall model comparison (Cases 1(iv)-2(iv)): (a) longitudinal profile of friction coefficient; (b)normalized $\overline{u'u'}$. Symbols: –⋆ –, free-slip; –□–, log-law; –◊–, no-slip; ◦, J and D experimental data.Note, error of experimental measurements has been denoted by error bars.

As expected, the free-slip condition is unable to resolve the near-wall velocity gradient within the inlet and recovery regions. Based on the $u(z)$ profile, the no-slip condition most accurately models the mean gradient of stream wise velocity near the wall. There are no significant differences in the $\overline{\overline{w}}(z)$ profiles.

There are no significant differences in the $\overline{w'w'}$ or $\overline{-u'w'}$ profiles. The $\overline{u'u'}$ profiles, shown in Figure 9b, experience the largest variations. The near-wall spike in $\overline{u'u'}$ in the inlet and recovery regions is not captured by any of the wall model cases. However, as previously discussed in 3.1.3, this is likely more dependent on grid resolution than the wall model. With all three models, $\overline{u'u'}$ is slightly over predicted near the surface in the recirculation and reattachment regions.

For the given computational domain, the no-slip condition and LES log-law model perform similarly. In the mean, the virtual measurement device closest to the wall is always within the linear sub layer of the LES wall model (z^+<12). Therefore, for both the log-law model and no-slip condition, $\partial\overline{u}/\partial z|_{z=0} = 0$ is calculated by a simple finite difference. Of note for the $h/\delta z$=10 resolution used in this study, within the inlet region the z^+ location of the virtual measurement device closest to the wall is always within the log layer. Additionally, within the recovery region, the device records occasional excursions into the log layer. The log-law model should, therefore, still be used for this case.

In addition to the placement of the virtual measurement device closest to the wall residing within the linear sub layer of the LES wall model, Le et al. concluded the vertical profile of velocity within the recirculation deviates from the log-law profile defined by the LES wall model. This is supported by present computational data, as shown in Figure 8. u^+ is observed to be independent of z^+ within the recirculation region, leading to significant deviations from the LES wall model specified u^+ profile. This leads to the no-slip condition being of similar, or greater, accuracy than the LES wall model for the given computational domain. Refer to Le et al. [5] for further details.

Conclusion

Large-eddy simulation of flow over a backward facing step is performed to study the effects of grid resolution, inlet turbulence conditions, eddy viscosity models, and wall boundary conditions. Computational results are compared to experimental data of Jovic and Driver [6].

The key finding of the present work is that, aside from grid resolution, specification of the mean profile and turbulence intensity at the inlet boundary is the most influential factor governing quality of

the downstream flow profiles. A grid resolution of $h/\delta z$=10 is adequate, although near-wall kinematic features and locations of turbulence RMS velocity extreme are more accurately represented with twice the resolution. Based on present FDS limitations, we conclude that with grid resolutions of $h/\delta z \geq 10$ the reattachment length may be predicted to within 10% (Table 1). The Deardorff and dynamic Smagorinsky reddy viscosity models produce very similar results. The no-slip wall condition and LES log-law model result in similarly accurate results due to the virtual measurement device closest to the wall residing within the wall model viscous sub layer (z^+ <12) in the mean in the post-step region. However, the LES log-law model is suggested to be the optimal wall boundary condition due to occasional instantaneous sampling in the log-law region.

Of note, the $h/\delta z$= 20 case performed worse for reattachment length in comparison to experimental data. The authors hypothesize this may be a manifestation of turbulence inlet profile specification limitations of FDS 6.1. However, the current study aims to present the simulations as is to compare the effects of various parameterization modifications, without modifying the LES code. Thus, while the authors recognize there is developmental work to be done on the Fire Dynamics Simulator that is not the aim of the current study.

For future work, inlet Reynolds stress specification should be studied to determine if this would be beneficial for matching experimental data near the inlet. Additionally, for the present study, specification of vertical profiles of inlet turbulence statistics is limited by the current FDS requirement that turbulence parameters are unique to each inlet. Modification of FDS to permit specification of inlet turbulence profiles should be considered.

Acknowledgment

This work was supported by the NIST Summer Undergraduate Research Fellowship (SURF) program.

References

1. Mc Grattan K, Hostikka S, McDermott R, Floyd J, Weinschek C, et al. (2014) Fire Dynamics Simulator Technical Reference Guide-1: Mathematical Model. NIST Special Publication 1018 Gaithersburg, Maryland.
2. McGrattan K, Hostikka S, McDermott R, Floyd J, Weinschek C, et al. (2013) FDS user's guide. NIST special Publication, 1019 Gaithersburg, Maryland.
3. Moon K, Hwang JM, Kim BG, Lee C, Choi J (2014) Large-eddy simulation of turbulent flow and dispersion over a complex urban street canyon. Environmental Fluid Mechanics.
4. Panjwani B, Ertesvag IS, Gruber A, Rian KE (2009) Large eddy simulation of backward facing step flow. In 5th National Conference on Computational Mech.
5. Le H, Moin P, Kim J (1997) Direct numerical simulation of turbulent flow over a backwardfacing step. Journal of Fluid Mechanics 330: 349-374.
6. Jovic S, Driver DM (1994) Backward-facing step measurements at low Reynolds number Re_h=5000 NASA Technical Memorandum108807.
7. Saric S, Jakirlic S, Tropea C (2005) A periodically perturbed backward-facing step flow by means of LES DES and t-rans. An example of flow separation control.
8. Kanna PR, Das MK (2009) Effect of geometry on the conjugate heat transfer of wall jet flow over a backward-facing step. J Heat Transfer 131.
9. Veturi R, Aung K (2005) A numerical study on mixing in turbulent flow behind a backwardfacing step. In ASME 2005 Fluids Engineering Division Summer Meeting 2.
10. Lee YT, Farabee TM, Blake WK (2007) Wall pressure fluctuations in the reattachment region of a backward facing step. In ASME/JSME 5thConference Joint Fluids Engineering 2.
11. Aider JL, Danet A (2006) Large-eddy simulation study of upstream boundary conditions influence upon a backward-facing step flow CR Mecanique 334: 447-453.
12. Sarwar M, Moinuddin KAM, Thorpe GR (2013) Large eddy simulation of flow over a backward facing step using fire dynamics simulator (fds) 14thAsian Congress of Fluid Mechanics 469-474.
13. Smagorinsky J (1963) General circulation experiments with the primitive equations. The basic experiment. Monthly Weather Review 91: 99-164.
14. Germano M, Piomelli U, Moin P, Cabot W (1991) A dynamic subgrid-scale eddy viscosity model physics of fluids 3: 1760-1765.
15. Germano M, Piomelli U, Moin P, Cabot W (1991) A dynamic subgrid-scale model for compressible turbulence and scalar transport physics of fluids 3: 2746-2757.
16. Deardorff JW (1972) Numerical investigation of neutral and unstable planetary boundary layers. Journal of Atmospheric Sciences 29: 91-115.
17. Vreman B (2004) An eddy-viscosity subgrid-scale model for turbulent shear flow. Algebraic Theory and Applications Phys Fluids 16: 3670-3681.
18. Jarrin N (2008) Synthetic inflow boundary conditions for the numerical simulation of turbulence PhD thesis. The University of Manchester.
19. Friedrich R, Arnal M (1990) Analyzing turbulent backward-facing step flow with the low pass filtered Navier-Stokes equations. Journal of Wind Engineering and Industrial Aerodynamics 38: 101-128.
20. Westphal RV, Johnston JP (1984) Effect of initial conditions on turbulent reattachment downstream of a backward facing step. AIAA121727-1732.
21. Pope SB (2000) Turbulent Flows. Cambridge University Press.